



Challenges associated with studying nonlinear distortion of acoustic waveforms emitted by high-speed jets

Woutijn J. BAARS¹; Charles E. TINNEY²; Mark F. HAMILTON³

¹ Department of Mechanical Engineering, The University of Melbourne, Melbourne, VIC 3010, Australia

² Center for Aeromechanics Research, The University of Texas at Austin, Austin, TX 78712, U.S.A.

³ Applied Research Laboratories, The University of Texas at Austin, Austin, TX 78713, U.S.A.

ABSTRACT

Discrepancies between linear predictions and direct measurements of the far-field sound produced by high-speed jet flows are typically ascribed to nonlinear distortion. Here we employ an effective Gol'dberg number to investigate the likelihood of nonlinear distortion in the noise fields of supersonic jets. This simplified approach relies on an isolated view of a ray tube along the Mach wave angle. It is known that the acoustic pressure obeys by cylindrical spreading in close vicinity to the jet before advancing to a spherical decay in the far-field. Therefore, a 'piecewise-spreading regime' model is employed in order to compute effective Gol'dberg numbers for these jet flows. Our first-principal approach suggests that cumulative nonlinear distortion can only be present within 20 jet exit diameters along the Mach wave angle when laboratory-scale jets are being considered. Effective Gol'dberg numbers for full-scale jet noise scenarios reveal that a high-degree of cumulative distortion can likewise be present in the spherical decay regime. Hence, full-scale jet noise fields are more affected by cumulative distortion.

Keywords: Jet Noise, Nonlinear Effects I-INCE Classification of Subjects Number(s): 21.6.1, 21.6.7/8

1. INTRODUCTION

Active noise suppression systems for high-speed jets will rely on real-time noise estimation procedures, and therefore, their control effectiveness depends on the accuracy of the underlying physical models. Despite over a half century of research with compelling progress, a full understanding has yet to be gleaned on how pronounced such nonlinear distortion effects are in the acoustic waveforms emitted by high-speed jets. A comprehensive review of the literature pertaining to this topic is beyond the scope of this paper. Albeit significant contributions include the work of Ffowcs Williams *et al.* (1), Pestorius & Blackstock (2), Crighton & Bashforth (3), Morfey & Howell (4), Petitjean *et al.* (5), Saxena *et al.* (6), Gee *et al.* (7) and Baars *et al.* (8) and the references therein.

It is common practice to categorize the noise features of supersonic jets according to their sound generating mechanism. This includes turbulent mixing noise, broadband shock-associated noise, screech and transonic resonance (9). Shock-free supersonic jets solely possess mixing noise induced by both fine-scale and large-scale turbulence within the jet's shear layer (10). When the convective speed of the turbulent large scales, U_c , becomes higher than the ambient sound speed a_∞ , a distinct region of high-intensity sound is produced that is concentrated in the post-potential core of the jet. The acoustic waves produced by these large scales radiate along the Mach wave angle $\phi = \cos^{-1}(a_\infty/U_c)$ and become more pronounced with increasing convective Mach number $M_c = U_c/a_\infty$. Figure 1 illustrates the acoustic field of an unheated and shock-free Mach 3 jet, as studied by Baars & Tinney (11), with a Mach wave angle of $\phi = 45^\circ$. The highest source intensity along the jet axis was identified to be at $x \approx 20D_j$, where x is the coordinate along the jet centerline and D_j is the jet exit diameter; r is the radial coordinate. The sound intensity is highest along the Mach wave angle (12, 13, 14), and thus, nonlinear distortion would be most pronounced there due to its high dependence on the sound intensity. For this reason we confine ourselves to an artificial ray tube drawn in Figure 1.

Cumulative nonlinear waveform distortion is commonly assumed to be a physical mechanism present in the sound field of supersonic jets. Discrepancies between predictions of the far-field sound (*e.g.* mapping near field spectra or waveforms) and direct measurements are often ascribed to nonlinear distortion when the far

¹wbaars@unimelb.edu.au

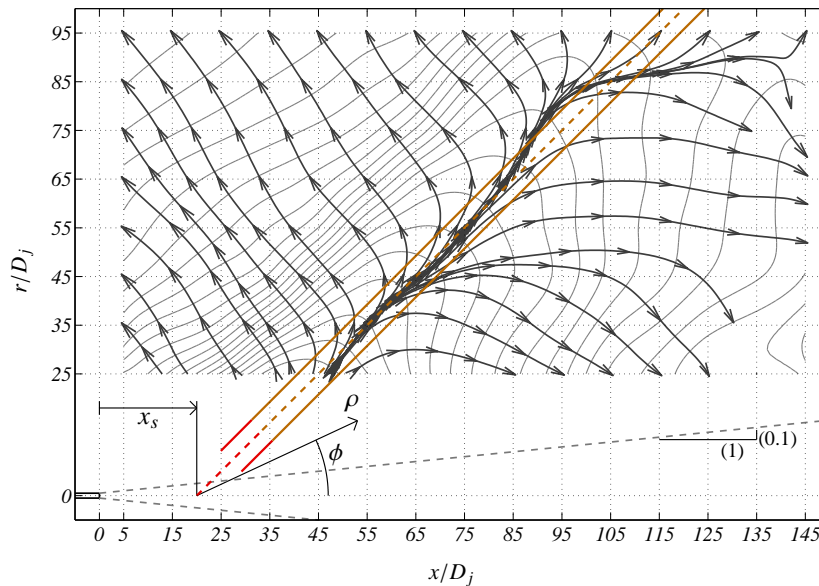


Figure 1 – Acoustic intensity field of a Mach 3 jet. Contours of OAPSL (grey isolines) are in dB *re* 20 μ Pa, taken from Baars & Tinney 2014 (11); highest level: 143 dB at $(x, r)/D_j \approx (45, 25)$, lowest level: 123 dB at $(x, r)/D_j \approx (10, 90)$, level step 1 dB. Field lines have an arbitrary starting point and spacing.

field signatures are predicted through geometric spreading and atmospheric absorption corrections alone. Especially when the discrepancy manifests itself at the high-frequency end of the spectrum, one is led to believe that the residuals between the predicted and measured spectra are attributed to nonlinear distortion. That is to say, cumulative waveform distortion includes waveform steepening, shock formation, shock coalescence and relaxation (15). The former, waveform steepening, is reflected in the spectrum by a shift of energy from mid frequencies to high frequencies (2). The cause of waveform steepening is the inherent effect of a change in particle velocity over the acoustic waveform that is dependent on the waveform's amplitude. The claim that the discrepancy between the predicted and measured spectra is caused by nonlinear distortion is exclusively valid if the physics provide conditions for the distortion to exist. Discrepancies can of course be caused by physical phenomena other than cumulative waveform distortion; other credible sources could be the complex interactions of waves in the near field, or the choice of an incorrect prediction path which is not aligned with the average propagation path. Moreover, a more compelling route to claim nonlinear distortion would be a prediction of the waveform (as opposed to the spectrum) through a nonlinear propagation algorithm (2). Once the predicted waveform matches the measured waveform and exhibits waveform steepening it is certain that cumulative nonlinear waveform distortion exists. A classic example of a high-speed jet study where steepened waveforms were believed not to be formed by nonlinear distortion can be found in the work of Ffowcs Williams *et al.* (1). During that study, personal communication between D. T. Blackstock and J. E. Ffowcs Williams (2) led them to the conclusion that amplitude levels at the source were simply too low for waveform steepening to exist. On the other hand, studies exist with convincing evidence for nonlinear distortion in the far field of the jet. For example, Gee *et al.* (7) showed that nonlinear waveform predictions in the far field, based on input waveforms closer to the jet, were a remarkable match to the measured waveforms in the far field of a full-scale jet engine, while linear predictions were unsatisfactory.

In the current study we assess the likelihood of there being nonlinear distortion in the noise fields of supersonic jets by employing effective Gol'dberg numbers. Recently, Baars *et al.* (8) explored the effective Gol'dberg number for a Mach 3 jet and concluded that their laboratory conditions were unfavourable to the accumulation of nonlinear distortion (the acoustic Mach number for this jet was 1.79). The effective Gol'dberg number is reviewed in § 2. A simple extrapolation model is then presented in § 3 to obtain relevant acoustic source characteristics for computing Gol'dberg numbers; § 4 presents effective Gol'dberg numbers for various supersonic jet noise studies.

2. REVIEW OF EFFECTIVE GOL'DBERG NUMBERS FOR DIVERGING WAVES

Recently, Hamilton (16) presented analytical expressions for effective Gol'dberg numbers applicable to cylindrically and spherically spreading wave fields. Here we provide a review of this work from the perspective of examining this number for jet aeroacoustics.

To determine the likelihood of cumulative nonlinear distortion, one must consider the relative strength of two competing effects: nonlinear distortion and energy absorption, the strengths of which are commonly expressed in terms of their individual length scales. We begin with expressions for planar wave fields, as the expressions for cylindrical and spherical spreading waves are based on this. The first length scale, the acoustic absorption length, is simply the reciprocal of the absorption coefficient, $l_a = 1/\alpha$, and reflects the strength of energy absorption. The second length scale, which is associated with nonlinear distortion, is the plane wave shock formation distance, and is defined as

$$\bar{x} = \frac{\rho_\infty a_\infty^3}{\beta(2\pi f_0) p_{\text{rms}}}, \quad (1)$$

where $\beta = (\gamma + 1)/2 = 1.2$ is the coefficient of nonlinearity for air, p_{rms} is the standard deviation of the acoustic pressure and f_0 is the characteristic frequency associated with the source.¹ The Gol'dberg number for planar waves is then defined as the ratio of the aforementioned length scales,

$$\Gamma = \frac{l_a}{\bar{x}}, \quad (2)$$

which appears naturally as the coefficient in front of the nonlinear term in the nondimensional form of the generalized Burgers equation (Hamilton & Blackstock (15), p. 312). For $\Gamma \lesssim 1$, attenuation dominates and the formation of shocks is suppressed. Conversely, when $\Gamma \gg 1$, cumulative nonlinear distortion is likely to occur. For jet noise applications, the representative acoustic signal at the source is relatively broadband; a hump resides which offers some relief when selecting a characteristic frequency for computing the Gol'dberg number. Finally, the frequency dependent absorption coefficient $\alpha(f)$ is taken at $f = f_0$ for a thermoviscous fluid with relaxation; see App. B of Blackstock (17).

Turning our attention now to diverging waves, *e.g.* cylindrical or spherical spreading fields, a third length scale is considered: the source radius r_0 , which is often expressed relative to the plane wave shock formation distance according to $\sigma_0 = r_0/\bar{x}$. While the evolution of a plane wave is determined completely by the single parameter Γ , two dimensionless parameters—length scale ratios Γ and σ_0 —determine the likelihood of nonlinear distortion in diverging wave fields. As reported by Hamilton (16), the *effective* Gol'dberg numbers for cylindrical waves and spherical waves are given by Eqs. (3a) and (3b), respectively.

$$\Lambda_c = \frac{\Gamma}{1 + \zeta_{sh}/(2\sigma_0)}, \quad (3a)$$

$$\Lambda_s = \Gamma \exp(-\zeta_{sh}/\sigma_0). \quad (3b)$$

Here, the constant ζ_{sh} is taken as $\zeta_{sh} = \pi/2$ and is motivated by the fact that Λ can now be interpreted in a similar manner as Γ from the perspective of the likelihood of cumulative nonlinear distortion to produce sawtooth waveforms. In this context, shock formation is guaranteed for $\Lambda \gg 1$, whereas nonlinear effects are suppressed and negligible for $\Lambda \lesssim 1$. It is important to mention that an underlying assumption for Eq. (3) is that the condition $k_0 r_0 \gg 1$ should be satisfied, where $k_0 = 2\pi f_0/a_\infty$. Finally, an independent nonlinear length scale to compute the shock formation distance for spherically diverging waves is used and is defined as: $\bar{r} = r_0 \exp(\sigma_0)$.

It is apparent from Eqs. (2), (3a) and (3b) that the Gol'dberg number is dependent on the source center frequency f_0 , amplitude p_{rms} and radius r_0 . As we will consider a collection of supersonic jet noise studies in this analysis, it is inevitable that f_0 , p_{rms} and r_0 will change such that the necessary conditions for nonlinear distortion are altered. For example, when a full-scale jet engine is geometrically scaled to a sub-scale size, as is commonly encountered in laboratory-environments, f_0 increases and r_0 decreases. The simplest scenario then is one that comprises aerodynamic similarity, such that the exit Mach number M_j , exit temperature ratio T_j/T_∞ and hence the exit velocity U_j , remain constant. In doing so, the Strouhal number remains constant ($\text{St}_{D_j} = f_0 D_j/U_j$), thereby allowing the center frequency to scale accordingly. Henceforth, frequency scales as $f_0 \propto 1/D_j$ while source size scales as $r_0 \propto D_j$. Furthermore, assuming that the acoustic source intensity is proportional to the exit velocity to a certain power b , then the source amplitude $p_{\text{rms}} \propto U_j^{b/2}$ should remain constant for an aerodynamically scaled jet. Unfortunately, under these assumptions, the effective Gol'dberg numbers for the full-scale and laboratory-scale study would not match. Thus for the *acoustics* part of study, the effective Gol'dberg number should ideally be of the same order of magnitude, or at least in the

¹Throughout this paper, Gol'dberg numbers are computed for standard temperature and pressure (STP) conditions of $p_\infty = 101,325$ Pa and $T_\infty = 293.15$ K; hence the ambient density and sound speed are $\rho_\infty = p_\infty/R/T_\infty$ and $a_\infty = \sqrt{\gamma R T_\infty}$, respectively.

same regime for scaled studies (e.g. $\Lambda \lesssim 1$ or $\Lambda \gg 1$)². It is important to emphasize the common practice of considering only similarity parameters such as M_j , T_j/T_∞ and Reynolds number Re_{D_j} when replicating a full-scale jet engine by way of laboratory-scale experiments. Thus, the effective Gol'dberg number is often overlooked as the parameters M_j , T_j/T_∞ and Re_{D_j} only govern the similarity of the *aerodynamics*. As was recognized previously (16), the Gol'dberg number can be interpreted as an acoustic Reynolds number and is equally imperative when using laboratory scale noise measurements to predict the acoustic waveforms produced by full-scale engines.

3. SUPERSONIC JET NOISE SOURCE CHARACTERISTICS

Here we present a simple extrapolation method in § 3.1 to obtain the acoustic source parameters necessary for computing effective Gol'dberg numbers using a ‘piecewise-spreading regime’ model; thereafter we apply this model to various high-speed jet noise studies from the literature (§ 3.2).

3.1 Extrapolation Model to Obtain Source Parameters

Defining the correct set of acoustic source parameters that represent the distribution of sources throughout the jet’s shear layer is challenging. It became evident that we require three source parameters for computing effective Gol'dberg numbers: the center frequency, the standard deviation of the acoustic pressure and the source radius. Furthermore, we confine ourselves to an artificial ray tube originating from the location of highest source intensity on the jet axis, that is oriented along the Mach wave angle (see Figure 1). We do this to encapsulate the correct propagation path of most intense sound generated by the convection of large-scale turbulence (18). To investigate the acoustic pressure decay along this ray tube we employ a wave packet model; its theoretical framework is discussed by Morris (18), Papamoschou (19) and others. Following the outline provided in App. A of Baars (20) and in Fiévet *et al.* (21), the pressure field resulting from the evolution of the jet’s large-scale instabilities are presented in Figure 1 and are necessary to estimate the acoustic pressure decay along the ray tube (coordinate ρ) as presented in Figure 2a. Laboratory measurements using 1/4 in. (11) and 1/8 in. microphones (21) are superimposed this wave packet model (corrected for atmospheric absorption based on STP and a relative humidity of 70%). It is important to mention that a wave packet length scale,

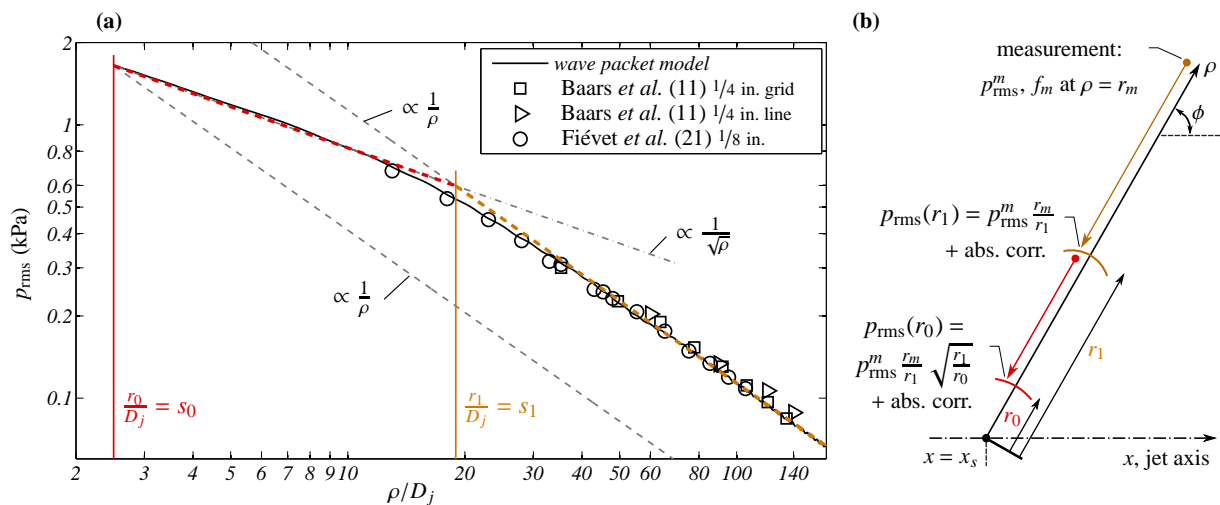


Figure 2 – (a) Pressure decay of the wave packet model fitted to the experimental measurements of Baars & Tinney (11) and Fiévet *et al.* (21). (b) Concept of simple extrapolation towards the source.

relative to the scale of the jet, had to be selected, which was denoted as parameter $A_1 = L/D_j$ (20). Here, L is the length scale of a wave packet comprising a harmonic wave with a Gaussian envelope $A(x) \propto \exp(-x^2/L^2)$. By fitting the wave packet model decay trend to the experimental data, the value of the wave packet parameter is found to be $A_1 = 8.75$. Thus, in close vicinity to the wave packet source, the acoustic pressure decay is shown to abide by cylindrical spreading ($p_{\text{rms}} \propto 1/\sqrt{\rho}$), while the pressure spreads spherically in the far field ($p_{\text{rms}} \propto 1/\rho$). To complete this ‘piecewise-spreading regime’ model we require a source radius r_0 and a range r_1 at which the decay transitions from cylindrical to spherical. Baars *et al.* (8) assumes that the source size is proportional to the jet diameter, $r_0 = s_0 D_j$, with a scale of $s_0 = 2.5$; this was driven by an estimated shear layer growth of $0.1x$ and a source location at $x \approx 20D_j$. The scale for location r_1 can be retrieved from Figure 2a

²The reader is referred to Baars *et al.* (8) for a more detailed discussion of the arguments supporting this scaling analysis.

and is approximately $s_1 = 19$. For this particular study, the pressure amplitudes at r_1 and r_0 were found to be $p_{\text{rms}}(r_1) = 598 \text{ Pa}$ and $p_{\text{rms}}(r_0) = 1,650 \text{ Pa}$, respectively. Note that the source amplitude is also presented in terms of overall sound pressure level (OASPL) throughout this paper: *i.e.* $\text{SPL}_0 = 20 \log(p_{\text{rms}}(r_0)/p_{\text{ref}})$ with $p_{\text{ref}} = 20 \mu\text{Pa}$. We now describe systematically how the source parameters at r_0 and r_1 are obtained using data provided in the open literature:

- To begin, a measure of the OASPL along the Mach wave angle is depicted and its acoustic amplitude is denoted as p_{rms}^m , where superscript ‘m’ refers to the measurement. Additionally, the peak in the sound pressure level (SPL) spectrum on a dB scale is identified as f_m . The measurement location $\rho = r_m$ along the Mach wave angle is computed through simple geometry from the location provided in the literature. That is, the source of the ray tube is assumed to reside at the location of highest source intensity $x_s = 10D_j$ (22, 23, 24), unless evidence for another location was provided; see Figure 2b for a schematic. Sporadically, the literature provides the A-weighted OASPL in dBA and hence it is imperative to obtain the unweighted OASPL in dB (see standard ANSI S1.6-1967 for the A weighting). Since the acoustic spectrum along the Mach wave angle is described by a Large Scale Similarity (LSS) spectrum (10) we can enforce the A-weighted LSS spectrum to obey by the OASPL value in dBA. Consequently, we obtain the OASPL in dB through the unweighted LSS spectrum; this is illustrated in Figure 3a for the study of Seiner *et al.* (25).

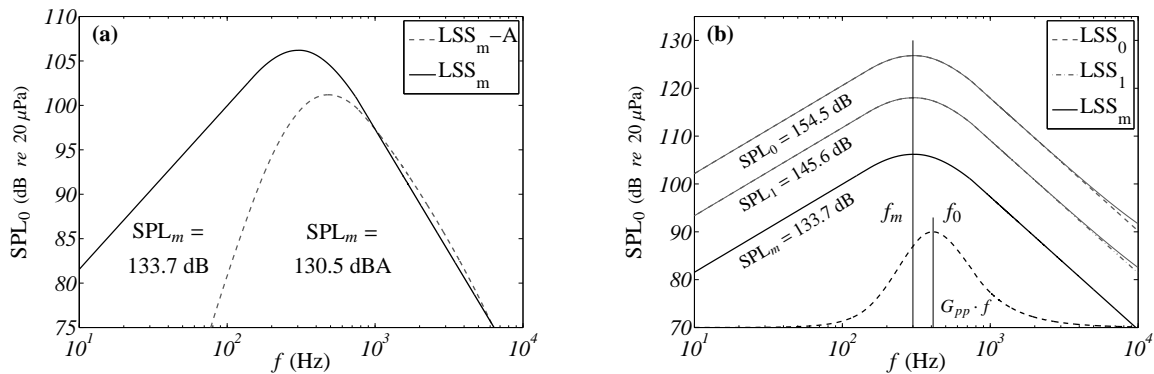


Figure 3 – (a) A-weighting applied to an acoustic LSS spectrum and (b) extrapolation procedure of LSS spectrum using geometric spreading and corrections for atmospheric absorption.

- Second, the measurement amplitude is extrapolated along the Mach wave angle to $\rho = r_1$ using spherical spreading and a correction for atmospheric absorption to reflect STP conditions and a relative humidity of 70%. The corrections are applied in the frequency domain to an LSS spectrum analogously to the dBA \rightarrow dB correction discussed above. Once the source amplitude $p_{\text{rms}}(r_1)$ is obtained, this extrapolation procedure is continued inwards using cylindrical geometric spreading towards source location r_0 to obtain $p_{\text{rms}}(r_0)$.
- Peak frequencies of the spectra are assumed to remain constant along the ray tube. However, characteristic frequencies f_0 and f_1 are taken as the peak frequency of the pre-multiplied LSS spectrum, as opposed to the SPL spectrum in dB scale. This can result in a center frequency that is 30% to 40% larger than f_m ; see the (arbitrary-scaled) pre-multiplied spectrum $G_{pp} \cdot f$ in Figure 3b that is analogous to the SPL spectrum identified as LSS_0 .

For now, $x_s = 10D_j$, $s_0 = 2.5$ and $s_1 = 19$ are assumed to be invariant with operating conditions of the supersonic jet. We recognize that this is a first-principal approach that relies on numerous simplifications. However, it is postulated that valuable insight into the likelihood of nonlinear distortion along the ray tube can still be gleaned through the computation of the Gol'dberg numbers based on these source parameters (§ 4). Omitting detailed intricacies of how x_s , s_0 and s_1 vary with operating conditions are unavoidable given that these relations are unknown. Moreover, the Gol'dberg number is an order-of-magnitude measure and so a sensitivity analyses of the results in § 4, to the choice of x_s , s_0 and s_1 , suggest that the current approach is reasonable. Also, note that solely changing s_0 would not result in a change in the source parameters at r_1 , while changing s_1 would alter the source parameters at both r_0 and r_1 . Nonetheless, future improvements are expected to be found in more accurate wave packet models since the choices of x_s , s_0 and s_1 are dependent on the wave packet analysis through, for example, parameter A_1 . And, beyond a doubt, near field temperature gradients, associated refraction phenomena, convection effects and near field interactions of acoustic waves from distributed sources within the jet affect the necessary complexity for a more accurate model.

3.2 Source Characteristics of Supersonic Jet Noise Studies

The model for obtaining source parameters at r_0 and r_1 is applied to various studies from the literature. Table 1 lists the selected high-speed jet studies with their most significant operating parameters, sorted according to scale. Source parameters at r_0 and r_1 are listed, as well as an indication as to whether the study was heated or unheated. Nine studies are considered as sub-scale, whereas seven studies correspond to full-scale jet engine scenarios. The latter category consists of one study comprising an isolated full-scale engine (25); remaining studies are concerned with fighter aircraft run-up studies (integrated systems). While operating

Table 1 – Source parameters and Gol'dberg numbers for supersonic jet noise studies.

study	scale				source parameters						Gol'dberg numbers			heated	marker
	D_j (cm)	M_j	T_j/T_∞	U_j (m/s)	SPL ₀ (dB)	f_0 (kHz)	$k_0 r_0$	SPL ₁ (dB)	$k_1 r_1$	Γ at r_0	Λ_c at r_0	Λ_s at r_1	\bar{r}_1/D_j		
Veltin <i>et al.</i> (26) [#]	1.27	1.75	0.62	473	150.8	6.1*	3.6	142.0	27	43	3.1	$6.6 \cdot 10^{-11}$	$> 10^8$	+	
Baars <i>et al.</i> (11)	2.54	3.00	0.35	610	158.9	4.9	5.7	150.1	43	130	35	$1.7 \cdot 10^{-1}$	$> 10^3$	×	
Petitjean <i>et al.</i> (5)	3.23	1.92	0.58	500	155.5	2.5*	3.6	146.7	28	125	15	$2.2 \cdot 10^{-5}$	$> 10^5$	□	
Petitjean <i>et al.</i> (5)	3.23	1.92	1.32	755	155.7	3.8*	5.6	146.9	43	106	20	$6.3 \cdot 10^{-3}$	$> 10^3$	✓ △	
Petitjean <i>et al.</i> (5)	3.23	1.92	1.65	844	155.7	4.2*	6.3	146.9	48	100	21	$1.5 \cdot 10^{-2}$	$> 10^3$	✓ □	
Baars <i>et al.</i> (27)	5.00	1.56	0.67	433	147.1	1.8	4.1	138.3	31	49	2.6	$6.1 \cdot 10^{-15}$	$> 10^{11}$	*	
Baars <i>et al.</i> (27)	5.00	1.56	2.40	820	155.8	3.4	7.8	147.0	60	114	30	$1.1 \cdot 10^{-1}$	$> 10^3$	✓ ☆	
Saxena <i>et al.</i> (6) [#]	6.22	1.90	1.65	835	153.5	2.0	5.8	144.7	44	101	16	$4.8 \cdot 10^{-4}$	$> 10^4$	✓ ◇	
Bridges (28)	10.2	1.50	1.52	636	151.6	1.1	5.1	142.8	39	76	8.3	$1.9 \cdot 10^{-6}$	$> 10^6$	✓ ○	
Seiner <i>et al.</i> (25) [#]	50.0	1.37	2.26	707	154.3	0.4	9.4	145.5	71	93	24	$9.2 \cdot 10^{-2}$	$> 10^3$	✓ ▽	
		single GE F404-400 engine, 95.5% ETR (F/A-18C/D aircraft)													
Saxena <i>et al.</i> (6)	50.0	F/A-18E AB on			163.2	0.5	12	154.4	95	253	196	39	62	✓ ◁	
		two integrated GE F414-400 engines engaged													
Gee <i>et al.</i> (29)	50.0	F/A-18E 100% ETR			161.4	0.5	12	152.6	95	205	135	20	82	✓ ▷	
		two integrated GE F414-400 engines engaged, one engine at idle													
Gee <i>et al.</i> (29)	50.0	F/A-18E AB on			165.4	0.5	12	156.6	95	324	298	76	48	✓ △	
		two integrated GE F414-400 engines engaged, one engine at idle													
Gee <i>et al.</i> (7)	75.0	F-22A 90% RPM			150.9	0.4	14	142.1	107	63	16	$6.6 \cdot 10^{-2}$	$> 10^3$	✓ ○	
		two integrated P&W F119 engines, one engine at idle													
Gee <i>et al.</i> (7)	75.0	F-22A AB on			156.1	0.4	14	147.3	107	114	51	2.6	209	✓ □	
		two integrated P&W F119 engines, one engine at idle													
Gee <i>et al.</i> (30)	95.0	F-35A 100% ETR			160.4	0.4	18	151.5	135	185	147	29	61	✓ ◇	
		single integrated P&W F135 engine													

conditions of laboratory-scale studies are generally well-documented, full-scale engine conditions are less accessible. A few remarks about the selected studies are now provided. For studies where f_0 is marked by ‘*’, no spectra were provided. Hence, f_0 was obtained through the assumption of a constant Strouhal number $St_{D_j} = 0.12$. Studies identified by ‘#’ were assumed to be conducted under STP conditions and a relative humidity of 70%. Regarding the full-scale studies, none of them were conducted under anechoic conditions. Therefore, corrections for ground reflections were sometimes applied by the authors, although surface properties (*e.g.* ground impedance) are an unknown factor when doing this. Finally, some aircraft run-up studies were performed with two engines operating simultaneously. Since the measurements were performed roughly in plane with both engines, the source diameter corresponding to a single engine was assumed. Furthermore, Gol'dberg numbers did not change more than one order of magnitude when varying D_j by a factor of two since a larger source size implies a lower source amplitude which will decrease Λ , but at the same time, a larger source will increase Λ .

4. EFFECTIVE GOL'DBERG NUMBER APPLIED TO SUPERSONIC JET NOISE

Insight into the values of the Gol'dberg numbers is provided in § 4.1, followed by an interpretation of the likelihood of nonlinear cumulative distortion for the selected high-speed studies in § 4.2.

4.1 Gol'dberg Number Ranges

Although acoustic waves throughout the ray tube exhibit cylindrical or spherical spreading, the Gol'dberg number for plane waves is considered first for reference. Isolines of constant Γ in the parameter space of source level (SPL₀) and frequency (f_0) are shown in Figure 4a. The markers indicate where the studies listed in Table 1 reside. It is important to realize to what extent relative humidity affects the absorption

coefficient and Gol'dberg number; this is illustrated in Figure 4b by isolines of $\Gamma = 100$ for different values of relative humidity. Now we focus on diverging waves. Since the acoustic pressure first decays cylindrically

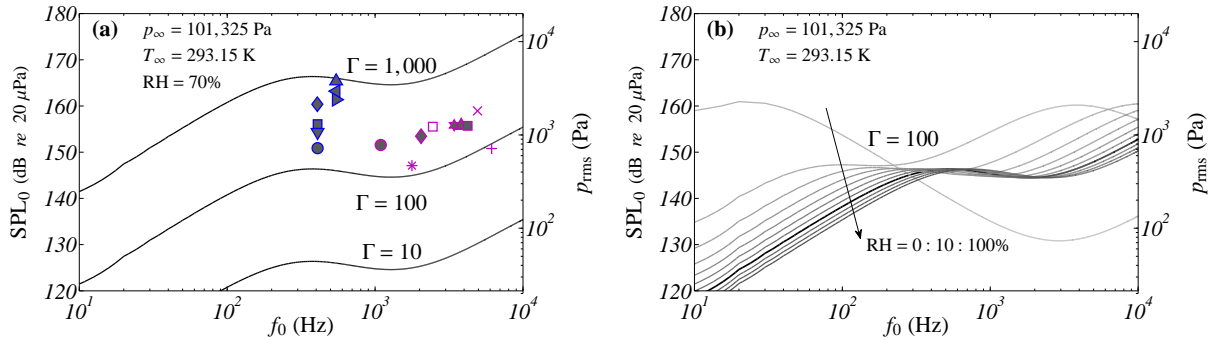


Figure 4 – Isolines of constant Gol'dberg numbers for planar wave fields. (a) Constant relative humidity of 70% and (b) varying relative humidity for two Gol'dberg numbers, $\Gamma = 1$ and $\Gamma = 100$.

($r_0 < \rho < r_1$), the Gol'dberg number Λ_c will be computed from source parameters at r_0 . Typical values of Λ_c in the parameter space of f_0 , SPL₀ and r_0 can be gleaned from Figure 5a. Alongside, in Figure 5c, source values at r_0 are visualized in the same parameter space. Following Table 1, blue markers represent sub-scale jet noise studies, while magenta markers correspond to full-scale studies; solid markers are associated with heated jets. Additionally, lines of constant $k_0 r_0 = 1$ & 10 are shown on the (f_0, r_0)-plane. If a jet study is scaled aerodynamically, the value of $k_0 r_0 \propto St_{D_j}$, since $r_0 \propto D_j$ and $f_0 \propto St_{D_j} U_j / D_j$. We further assume that St_{D_j} is constant and that the sound intensity SPL₀ is similar for the scaled scenario, since U_j is invariant. This implies that for this ideal scaling scenario we would move along a line of constant $k_0 r_0$; the markers in Figure 5c support this. The scatter is caused by the change in operating conditions and associated variations in Strouhal number. One can also visually observe why effective Gol'dberg numbers are expected to change when scaling jets: isosurfaces of constant Λ_c do not correspond to the constant values of $k_0 r_0$ (Figure 5a).

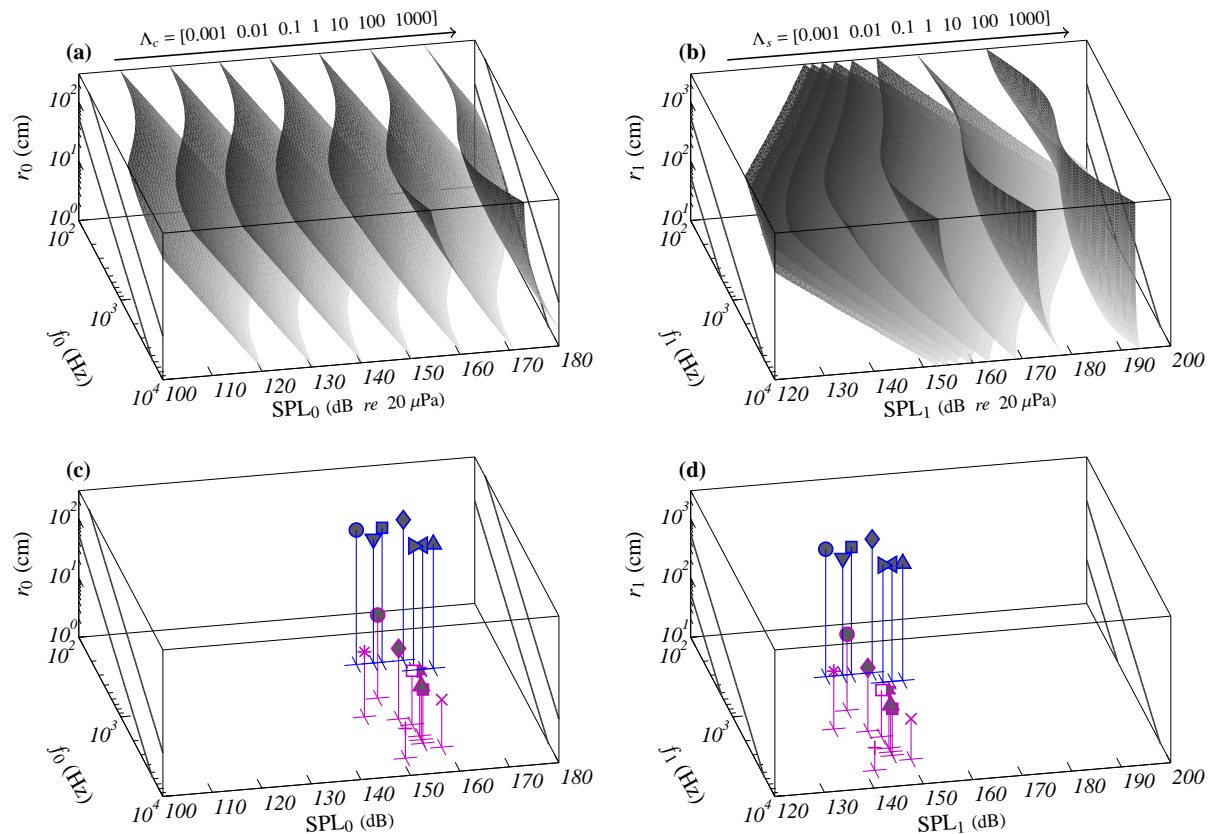


Figure 5 – (a,b) Isosurfaces of constant Gol'dberg numbers for (a) cylindrical and (b) spherical waves; STP and rel. hum. of 70%. (c,d) Source parameters listed in Table 1 for (c) source r_0 and (d) source r_1 .

Since spherical spreading holds for $\rho > r_1$, the effective Gol'dberg number for spherical diverging waves is computed from source parameters at r_1 : $\Lambda_s = \Lambda_s(f_1, \text{SPL}_1, r_1)$. Isosurfaces of constant Λ_s , as well as the r_1 source parameters, are shown in Figures 5b and 5d, respectively. As seen for the planar Gol'dberg number, the relative humidity has a significant influence on the Gol'dberg number and hence the existence of nonlinear distortion. Figures 6a and 6b show isosurfaces for $\Lambda = 1$ & 100 for a relative humidity of 0% to 100%. As expected, under similar source conditions, the Gol'dberg number becomes higher when the relative humidity increases from 10% to 100%, since the absorption coefficient decreases when $f < 5$ kHz (true for almost all studies considered). Realistically, effective Gol'dberg numbers can change up to one order of magnitude for the most extreme variations in humidity. The practical consequence is that the same fighter aircraft operating in a dry desert is more likely to trigger nonlinear distortion than one that is operating in a humid, tropical climate.

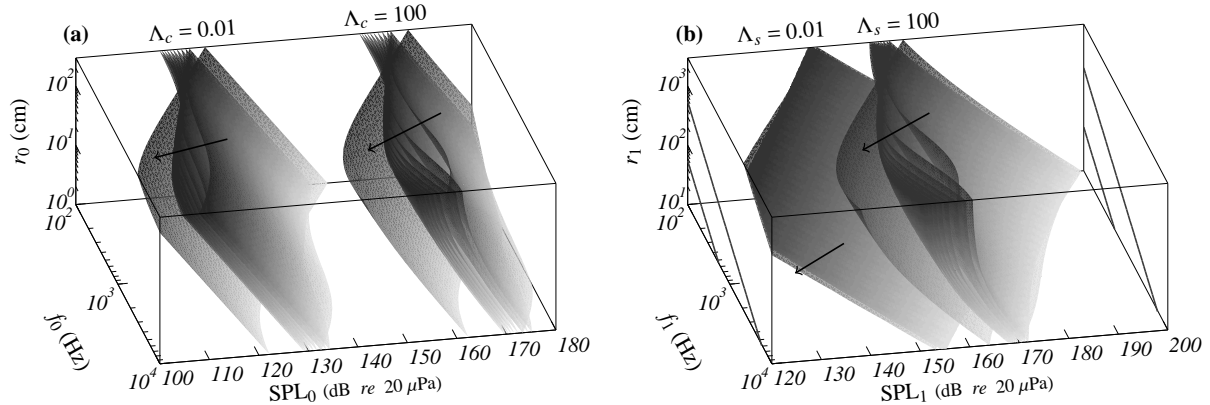


Figure 6 – Isosurfaces of constant effective Gol'dberg numbers $\Lambda = 0.01$ and $\Lambda = 100$ for (a) cylindrical and (b) spherical wave fields for varying relative humidities: 0 \rightarrow 100% (step size 10%).

4.2 Quadrants of Effective Gol'dberg Number

We have now arrived at a detailed look at the values of Λ_c and Λ_s . Each study is visualized in the (Λ_c, Λ_s) -plane in Figure 7a alongside a schematic in Figure 7b that illustrates where effective Gol'dberg numbers were calculated. Four quadrants appear from the criterion that nonlinear distortion is suppressed for $\Lambda \leq 1$ and likely to be pronounced for $\Lambda \gg 1$. All considered sub-scale studies populate quadrant 2, meaning that

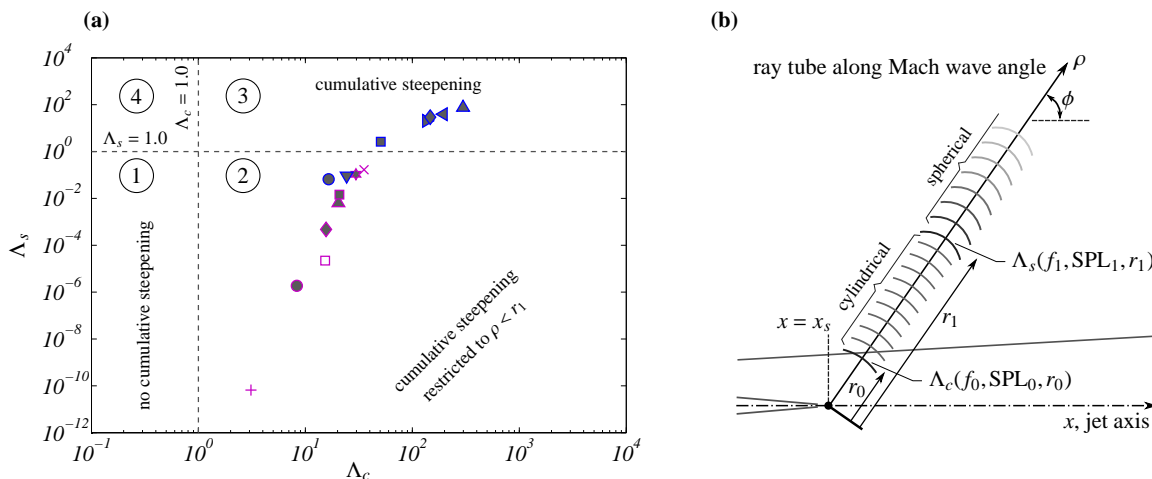


Figure 7 – (a) Effective Gol'dberg numbers for cylindrical and spherical waves for the studies listed in Table 1. (b) Schematic of the acoustics along the ray tube for interpretation of the effective Gol'dberg numbers.

cumulative waveform steepening can occur in the cylindrical regime ($r_0 < \rho < r_1$) but that it will be absent when spherical spreading takes over ($\rho > r_1$), and so, cumulative waveform steepening can only occur in close vicinity to the jet. Five of the seven full-scale jet studies lay in quadrant 3, which suggests that cumulative steepening occurs in both the cylindrical and spherical spreading regime. Two full-scale studies are exceptions and reside in quadrant 2. The first of these, by Seiner *et al.* (25), was performed using a single engine operating at 95.5% ETR and had a lower exit Mach number and exit velocity than its sub-scale counterpart (27) and

other full-scale studies. The study by Gee *et al.* (7) on the F-22A operating at 90% RPM (intermediate thrust setting) also resides in quadrant 2. They showed waveforms along the Mach wave angle in the domain that we identify by $\rho > r_1$, but whether these exhibit waveform steepening is questionable. When this same integrated engine is ramped up to higher thrust settings with afterburners (AB) engaged, waveform steepening was observed by Gee *et al.* (7) for $\rho > r_1$, which agrees with our values of the effective Gol'dberg number.

5. CONCLUSIONS

Studying and interpreting nonlinear cumulative distortion effects in noise fields of supersonic jets is challenging when various experimental scales are considered. Here we employed the effective Gol'dberg number to investigate the likelihood of nonlinear waveform steepening along the Mach wave angle of jets with supersonic convective Mach numbers. We emphasized the importance of this effective Gol'dberg number as a nondimensional similarity parameter that has to be considered when one is interested in studying a representative degree of full-scale nonlinear distortion in a laboratory-scale environment. Our analysis suggests that nonlinear distortion can only be pronounced within 20 jet exit diameters along the Mach wave angle, when laboratory-scale jets are concerned. Effective Gol'dberg numbers for full-scale jets reveal that a high degree of cumulative distortion can also reside beyond $\rho = 20D_j$, where the acoustic pressure experiences spherical spreading. Therefore, full-scale jet noise fields are relatively more affected by cumulative distortion.

ACKNOWLEDGEMENTS

The authors wish to acknowledge support from the Office of Naval Research, ONR award number N00014-11-1-0752, with Dr. Joseph Doychak and Dr. Brenda Henderson as program managers. WJB would like to acknowledge the Australian Research Council for funding his current position at the University of Melbourne.

REFERENCES

1. Ffowcs Williams JE, Simson J, Virchis VJ. 'Crackle': an annoying component of jet noise. *J Fluid Mech.* 1975;71:251–271.
2. Pectorius FM, Blackstock DT. Propagation of finite-amplitude noise. In: *Finite-amplitude wave effects in fluids*, Proc. of 1973 Symp. Copenhagen, Denmark: IPC Science and Tech. Press Ltd; 1974. p. 24–29.
3. Crighton DG, Bashforth S. Nonlinear propagation of broadband jet noise. In: *6th AIAA Aeroacoustics Conf.*, paper 1980-1039. AIAA; 1980. p. 1–8.
4. Morfey CL, Howell GP. Nonlinear propagation of aircraft noise in the atmosphere. *AIAA J.* 1981;19(8):986–992.
5. Petitjean BP, Viswanathan K, McLaughlin DK. Acoustic pressure waveforms measured in high speed jet noise experiencing nonlinear propagation. *Intl J Aeroacous.* 2006;5(2):193–215.
6. Saxena S, Morris PJ, Viswanathan K. Algorithm for the nonlinear propagation of broadband jet noise. *AIAA J.* 2009;47(1):186–194.
7. Gee KL, Sparrow VW, James MM, Downing JM, Hobbs CM, Gabrielson TB, et al. The role of nonlinear effects in the propagation of noise from high-power jet aircraft. *J Acoust Soc Am.* 2008;123(6):4082–4092.
8. Baars WJ, Tinney CE, Wochner MS, Hamilton MF. On cumulative nonlinear acoustic waveform distortions from high-speed jets. *J Fluid Mech.* 2014;749:331–366.
9. Tam CKW. Supersonic jet noise. *Annu Rev Fluid Mech.* 1995;27:17–43.
10. Tam CKW, Golebiowski M, Seiner JM. On the two components of turbulent mixing noise from supersonic jets. In: *2nd AIAA/CEAS Aeroacoustics Conf.*, paper 1996-1716. AIAA; 1996. p. 1–17.
11. Baars WJ, Tinney CE. Shock-structures in the acoustic field of a Mach 3 jet with crackle. *J Sound Vib.* 2014;333(12):2539–2553.
12. Phillips OM. On the generation of sound by supersonic turbulent shear layers. *J Fluid Mech.* 1960;9:1–28.
13. Seiner JM, Bhat TRS, Ponton MK. Mach wave emission from a high-temperature supersonic jet. *AIAA J.* 1994;32(12):2345–2350.

14. Tam CKW, Chen P. Turbulent mixing noise from supersonic jets. *AIAA J.* 1994;32(9):1774–1780.
15. Hamilton MF, Blackstock DT, eds. *Nonlinear acoustics*. Melville, NY: ASA; 2008.
16. Hamilton MF. Effective Gol'dberg number for diverging waves. *J Acoust Soc Am.* 2013;134(5):4099.
17. Blackstock DT. *Fundamentals of physical acoustics*. New York, NY: Wiley; 2000.
18. Morris PJ. A note on noise generation by large scale turbulent structures in subsonic and supersonic jets. *Intl J Aeroacous.* 2009;8(4):301–316.
19. Papamoschou D. Wavepacket modeling of the jet noise source. In: 17th AIAA/CEAS Aeroacoustics Conf., paper 2011-2835. AIAA; 2011. p. 1–20.
20. Baars WJ. *Acoustics from high-speed jets with crackle*. The University of Texas at Austin. TX; 2013.
21. Fiévet R, Tinney CE, Baars WJ, Hamilton MF. Acoustic waveforms produced by a laboratory scale supersonic jet. In: 20th AIAA/CEAS Aeroacoustics Conf., paper 2014-2906. AIAA; 2014. p. 1–20.
22. Hileman JI, Thurow BS, Caraballo EJ, Samimy M. Large-scale structure evolution and sound emission in high-speed jets: real-time visualization with simultaneous acoustic measurements. *J Fluid Mech.* 2005;544:277–307.
23. Kuo CW, Veltin J, McLaughlin DK. Effects of jet noise source distribution on acoustic far-field measurements. *Intl J Aeroacous.* 2012;11(7-8):885–915.
24. James MM, Salton AR, Gee KL, Neilsen TB, McInerny SA, Kenny RJ. Modification of directivity curves for a rocket noise model. In: 164th Meeting of the ASA., Vol. 18, 040008. ASA; 2014. p. 1–13.
25. Seiner JM, Ukeiley LS, Jansen BJ. Aero-performance efficient noise reduction for the F404-400 engine. In: 11th Aeracoustics Conf., paper 2005-3048. AIAA/CEAS; 2005. p. 1–13.
26. Veltin J, Day BJ, McLaughlin DK. Correlation of flowfield and acoustic field measurements in high-speed jets. *AIAA J.* 2011;49(1):150–163.
27. Baars WJ, Tinney CE, Murray NE, Jansen BJ, Panickar P. The effect of heat on turbulent mixing noise in supersonic jets. In: 49th Aerospace Sciences Meeting, paper 2011-1029. AIAA; 2011. p. 1–14.
28. Bridges JE. Broadband shock noise in internally-mixed dual-stream jets. In: 15th AIAA/CEAS Aeroacoustics Conf., paper 2009-3210. AIAA; 2009. p. 1–17.
29. Gee KL, Gabrielson TB, Atchley AA, Sparrow VW. Preliminary analysis of nonlinearity in military jet aircraft noise propagation. *AIAA J.* 2005;43(6):1398–1401. Technical note.
30. Gee KL, Downing JM, James MM, McKinley RC, McKinley RL, Neilsen TB, et al. Nonlinear evolution of noise from a military jet aircraft during ground run-up. In: 18th AIAA/CEAS Aeroacoustics Conf., paper 2012-2258. AIAA; 2012. p. 1–13.